

Origin of quasi-flat bands in phosphorene nanoribbons: A tight-binding calculation

PROJECT REPORT
COMPUTATIONAL PHYSICS
PH-354

BY

HARSHVARDHAN SINGH DEORA
INTEGRATED PhD PROGRAMME
CHEMICAL SCIENCE DEPARTMENT
INDIAN INSTITUTE OF SCIENCE



UNDER THE SUPERVISION OF
PROF. AWADHESH NARAYAN
SOLID STATE AND STRUCTURAL CHEMISTRY UNIT
INDIAN INSTITUTE OF SCIENCE

Abstract

In this investigation, we conducted a comprehensive analysis of the band structure, state characterization, and Quantum electronic transport properties of monolayer black phosphorus (phosphorene) zigzag nanoribbons (zPNRs) and armchair nanoribbons (aPNRs) using a five-parameter tight-binding (TB) approximation. The results which we are replicating were published by Sisakht et al. [1]. We started with 4 band model and 2 band model of monolayer phosphorene to observe the massless fermions along the armchair direction and then move to its nanoribbons where we calculated their band structures for three different ratios of $|t_2/t_1|$ and concluded that at $|t_2/t_1| > 2$, zPNRs show non-trivial topological state due to emergence of edge states. Then we performed calculations to understand the effect of in plane external electric field along the ribbon width on the band structure and probability amplitude of the sites in the nanoribbons. In the end, we calculated Transmission of electrons through 10-zPNR to understand it's electronic transport nature. We calculated Transmission of 2 different systems: (a) Square lattice as both device and leads, (b) 10-zPNR as both device and leads.

Contents

Abstract	1
1 Exploration of Phosphorene monolayer	1
1.1 Introduction	1
1.2 Model Hamiltonian	2
1.2.1 Four band model	2
1.2.2 Two band model	5
1.3 Phosphorene nanoribbons	6
1.3.1 Zigzag nanoribbon	6
1.3.2 Armchair nanoribbon	12
1.4 Effect of in-plane External electric field	14
1.4.1 Response of aPNR to E_{ext}	14
1.4.2 Response of zPNR to E_{ext}	18
1.5 Quantum transport in zig-zag nanoribbon	21
1.5.1 Landauer-Buttiker Formalism for square lattice	21
1.5.2 Transmission in Square Lattice arrangement	24
1.5.3 Transmission in 10-zPNR	24
1.6 Conclusion	26

Chapter 1

Exploration of Phosphorene monolayer

1.1 Introduction

Graphene, a material of immense interest discovered in recent years, exhibits unique properties governed by massless Dirac fermions in its low-energy theory, resulting in exceptional electrical characteristics. In applications relevant to semiconductor technology, the necessity arises for a discernible band gap that restricts electron mobility. Notably, armchair graphene nanoribbons demonstrate gap formation correlated with their dimensions, and bilayer graphene subjected to a perpendicular electric field similarly manifests a band gap^[2]. It is desirable to find an atomic monolayer bulk sample that has a finite gap.

A rising contender in the realm of post-graphene materials is phosphorene, characterized by a honeycomb structure derived from black phosphorus. Its successful synthesis in laboratory settings has been documented, highlighting its considerable promise in electronic applications. Black phosphorus, a layered material, features atomic layers held together by Van der Waals forces. Similar to the isolation of graphene from graphite, phosphorene can be obtained via the mechanical exfoliation technique from black phosphorus. Its fundamental structure deviates from planarity, exhibiting a puckered configuration owing to sp^3 hybridization, as depicted in Fig 1.1.

An intriguing feature of phosphorene nanoribbons is the emergence of a quasi-flat edge band that remains distinct from the bulk band structure. In this report, our investigation delves into the band characteristics of phosphorene nanoribbons through numerical approaches. Drawing parallels with graphene, where electron hopping occurs between first-nearest neighbor sites with $t_1 = t_2 = 1$ and $t_3, t_4, t_5 = 0$, we find that the origin of the flat bands in graphene is attributed to topological considerations. Extending this reasoning to phosphorene, we demonstrate the genesis of the quasi-flat edge band. Specifically, the interplay between the ratio $|t_2/t_1|$ and the parameter t_4 assumes critical significance: the quasi-flat bands become detached from the bulk band structure when the ratio attains a value of 2, while the presence of transfer energy t_4 induces bending in these flat bands. We will also understand the effect of in-plane external electric field along the width of the phosphorene nanoribbons.

The results which I am replicating are from [1].

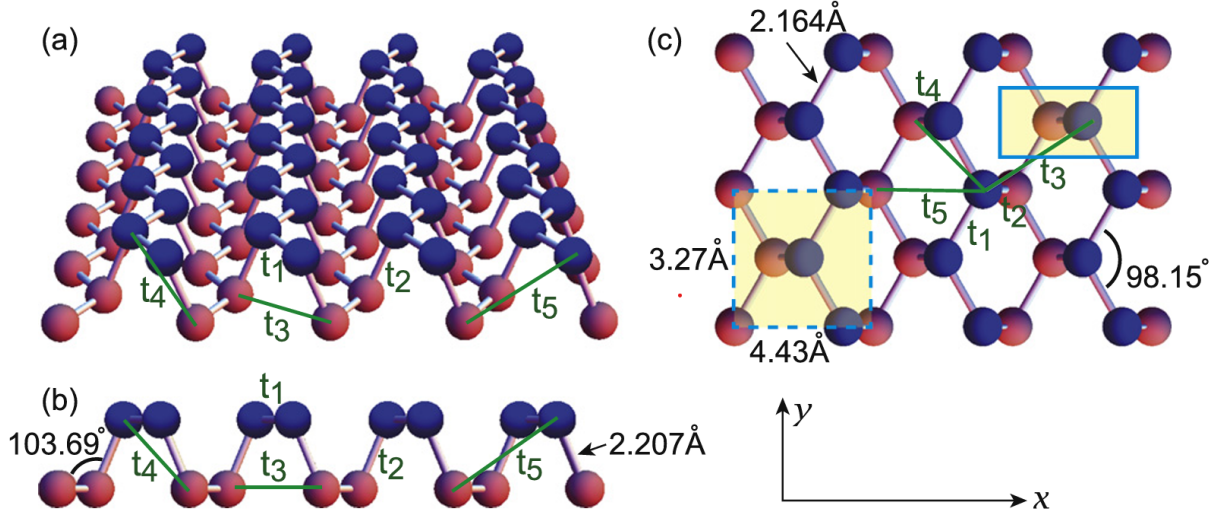


Figure 1.1: This figure shows structure of monolayer phosphorene with five nearest neighbour hopping interals. Adapted from ref [3].

1.2 Model Hamiltonian

The tight-binding model is given by

$$\mathbf{H} = \sum_{\langle i,j \rangle} t_{ij} c_i^\dagger c_j \quad (1.1)$$

Here summation is over lattice sites, t_{ij} is hopping from i^{th} site to j^{th} site and $c_i^\dagger (c_j)$ is the creation(annihilation) operator of electrons at site i(j). We will consider five nearest hopping here: $t_1 = 1.22$ eV, $t_2 = -3.66$ eV, $t_3 = 0.205$ eV, $t_4 = 0.105$ eV, $t_5 = 0.055$ eV.

1.2.1 Four band model

In Fig 1.2, the unit cell of a monolayer of phosphorene is depicted as a rectangle comprising four phosphorus atoms.

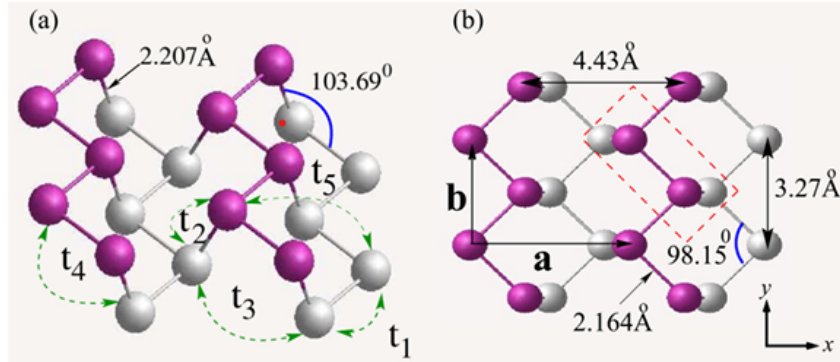


Figure 1.2: This figure shows structure of monolayer phosphorene with red color box showing the unit cell. Adapted from ref [1].

The Fourier-transformed general Hamiltonian in momentum space can be expressed as follows:

$$\mathbf{H} = \sum_k \Psi_k^\dagger \mathbf{H}_k \Psi_k \quad (1.2)$$

where $\Psi_k^\dagger = (a_k^\dagger b_k^\dagger c_k^\dagger d_k^\dagger)$ and \mathbf{H}_k is a 4 x 4 matrix

$$\mathbf{H}_k = \begin{pmatrix} 0 & A_k & B_k & C_k \\ A_k^* & 0 & D_k & B_k \\ B_k^* & D_k^* & 0 & A_k \\ C_k^* & B_k^* & A_k^* & 0 \end{pmatrix} \quad (1.3)$$

where we are keeping onsite energies as 0 and

$$\begin{aligned} A_k &= t_2 + t_5 e^{-ik_a} \\ B_k &= 4t_4 e^{-i\frac{(k_a-k_b)}{2}} \cos\left(\frac{k_a}{2}\right) \cos\left(\frac{k_b}{2}\right) \\ C_k &= 2e^{i\frac{k_b}{2}} \cos\left(\frac{k_b}{2}\right) (t_1 e^{-ik_a} + t_3) \\ D_k &= 2e^{i\frac{k_b}{2}} \cos\left(\frac{k_b}{2}\right) (t_3 e^{-ik_a} + t_1) \end{aligned} \quad (1.4)$$

Here $k_a = \mathbf{k} \cdot \mathbf{a} \hat{\mathbf{x}}$ and $k_b = \mathbf{k} \cdot \mathbf{b} \hat{\mathbf{y}}$ where $\mathbf{a} \hat{\mathbf{x}}$ and $\mathbf{b} \hat{\mathbf{y}}$ are primitive lattice vectors of the structure.

Since,

$$\begin{aligned} \mathbf{k}_x &= \frac{2\pi q_x}{a} \\ \mathbf{k}_y &= \frac{2\pi q_y}{b} \end{aligned} \quad (1.5)$$

Then

$$\begin{aligned} k_a &= \mathbf{k} \cdot \mathbf{a} \hat{\mathbf{x}} = 2\pi q_x \\ k_b &= \mathbf{k} \cdot \mathbf{b} \hat{\mathbf{y}} = 2\pi q_y \end{aligned} \quad (1.6)$$

where q_x and q_y goes from -0.5 to +0.5.

So, if we diagonalize the Hamiltonian in eq 1.3 on a grid of k_a and k_b on a path of high symmetry points, then we expect 4 eigen values at each k-point and plotting them give us band structure of 4 band model of monolayer phosphorene which can be seen in Fig 1.3.

In Fig 1.3, we can see that the band dispersion is highly relativistic along $\Gamma \rightarrow X$ direction and non-relativistic(parabolic) along $\Gamma \rightarrow Y$ direction near the conduction band minima and valence band maxima. It means the effective mass of fermions moving along $\Gamma \rightarrow X$ will be very less as compared to fermions moving along $\Gamma \rightarrow Y$ direction or we can also say electrons and holes moving along zigzag direction are heavier than those moving along armchair direction. The conduction band and valence band are like mirror image of each other because of sub-lattice symmetry present in the hamiltonian.

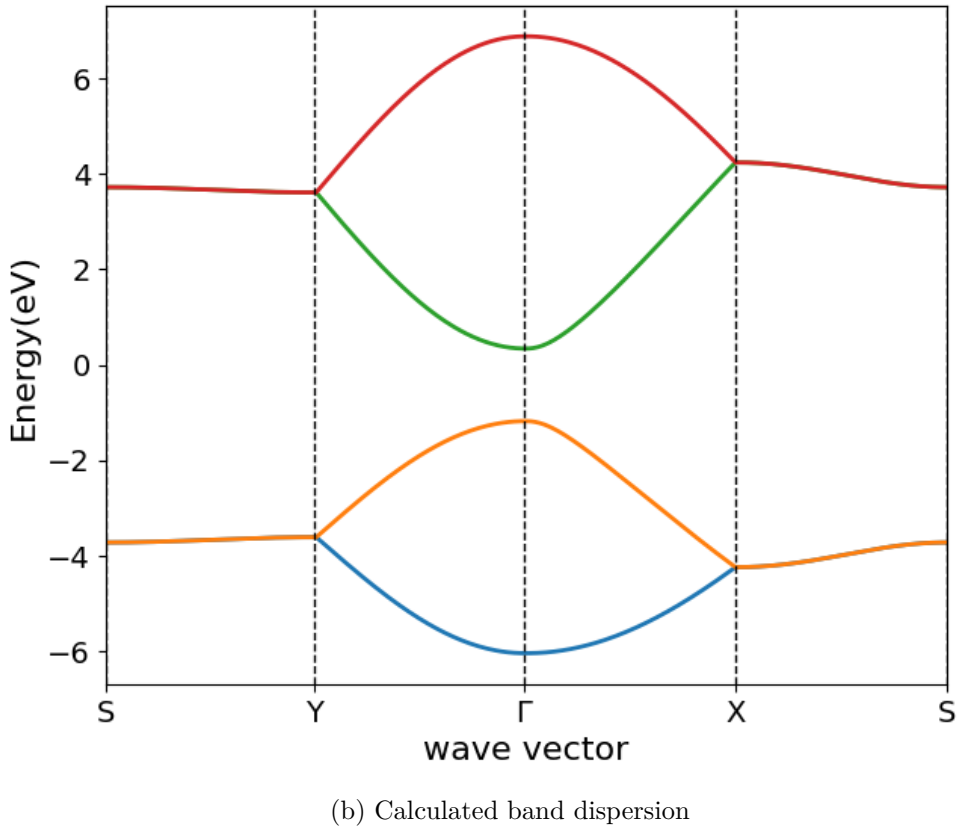
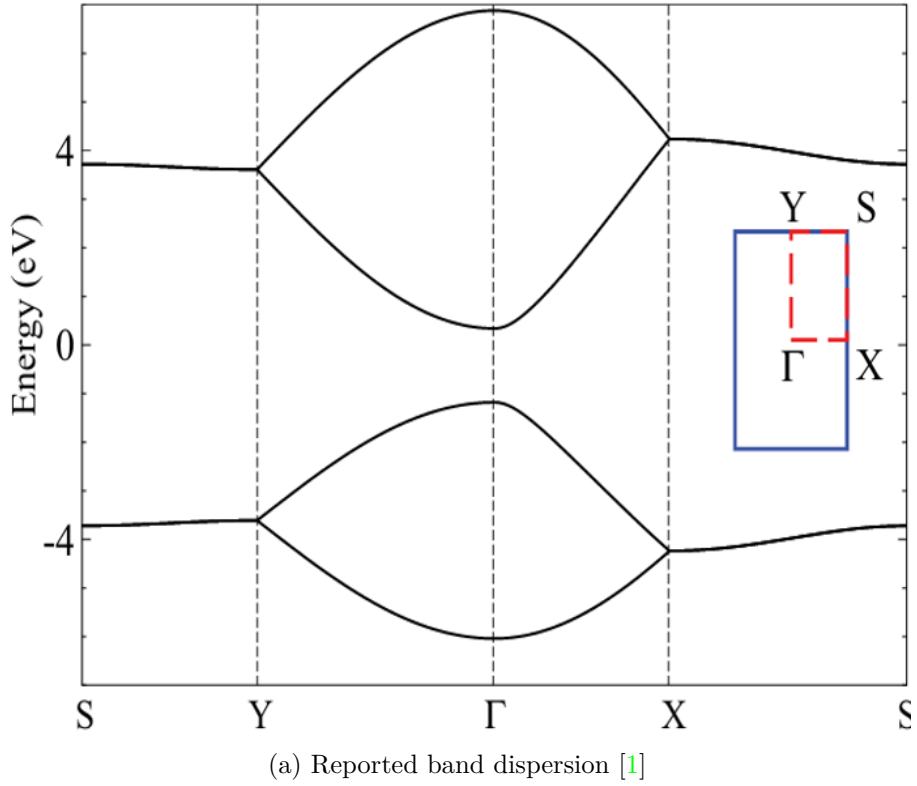


Figure 1.3: This Figure shows the band structure, of 4 band model along high symmetry path S → Y → Γ → X → S.

1.2.2 Two band model

In the TB Hamiltonian of Eq.1.1, if we project the positions of the upper and lower zigzag chains on a horizontal plane and keep the previous hopping integrals, the unit cells of the electronic system is reduced to two phosphorus atoms per unit cell. The Fourier transform of the resulting two band model is given by

$$\mathbf{H} = \sum_k \phi_k^\dagger \mathbf{H}_k \phi_k \quad (1.7)$$

where $\phi_k^\dagger = (a_k^\dagger b_k^\dagger)$ and \mathbf{H}_k is a 2 x 2 matrix

$$\mathbf{H}_k = \begin{pmatrix} B_k e^{i\frac{(k_a-k_b)}{2}} & A_k + C_k e^{i\frac{(k_a-k_b)}{2}} \\ A_k^* + C_k^* e^{-i\frac{(k_a-k_b)}{2}} & B_k e^{i\frac{(k_a-k_b)}{2}} \end{pmatrix} \quad (1.8)$$

Again diagonalizing this matrix on same high symmetry path as in four band model gives us the band structure shown in Fig 1.4.

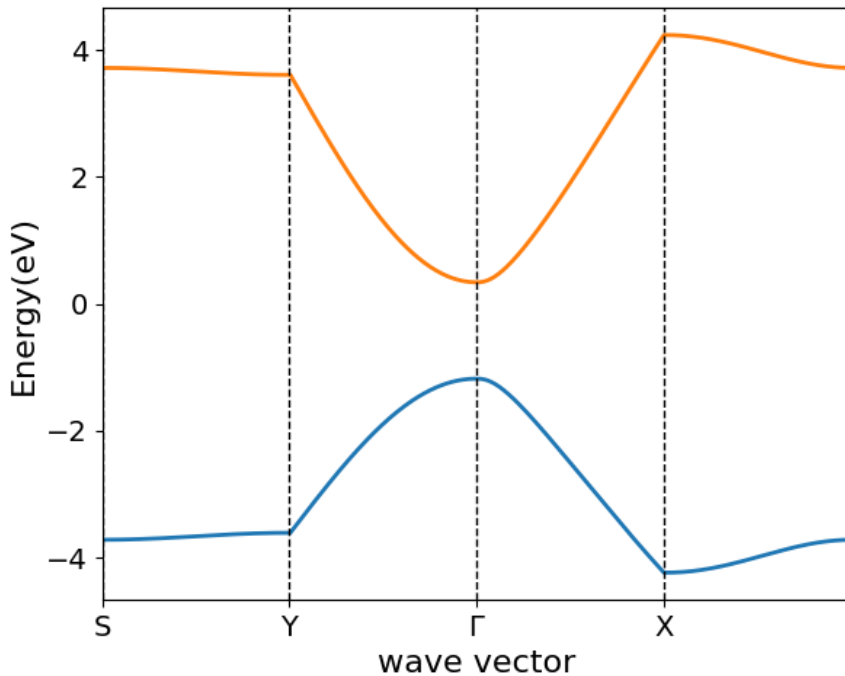


Figure 1.4: This Figure shows the band structure, of 2 band model along high symmetry path S → Y → Γ → X → S. Note-The paper which we are replicating didn't show the band structure of 2 band model. They just gave the Hamiltonian for it. We are just showing it because we did it.

If you want to see the projection in the horizontal plane, you can refer to Fig 1.6a where we will discuss about nanoribbons. You can think it as a bulk material and unit cell will have 2 atoms in it connected by black bonds that can be translated to complete the lattice arrangement.

1.3 Phosphorene nanoribbons

In the forthcoming numerical analysis, we aim to elucidate the electronic characteristics of two distinct types of nanoribbons: zig-zag nanoribbon and armchair nanoribbon. These nanoribbons are differentiated based on the orientation of their periodicity. In these nanoribbons, the structure of aPNR (armchair Phosphorene nanoribbon) is defined by the number of dimer lines across the ribbon width (N_a -aPNRs), whereas that of zPNR is defined by the number of zigzag chains across the ribbon width (N_z -zPNRs).

To compute the band structure and eigenstates of the nanoribbons, we derive the eigenvalues and eigenvectors of the matrix representing the crystal Hamiltonian between Bloch sums:

$$\mathbf{M}_{\alpha\beta} = - \sum_{ij} t_{i\alpha;j\beta} e^{i\mathbf{k}\cdot\mathbf{R}_{ij}} \quad (1.9)$$

where i and j denote different unit cells, α and β denote the basis sites in a unit cell. Further, \mathbf{k} is the wave vector, and R_{ij} represents a Bravais lattice vector. Moreover, $t_{i\alpha;j\beta}$ are the hopping integrals between the basis site α of unit cell i and the basis site β of unit cell j , and will be substituted by the five hopping parameters of the model, accordingly. In nanoribbons, the periodicity is confined to the ribbon's length, resulting in a number of basis sites within each unit cell that scales proportionally with the ribbon's width.

1.3.1 Zigzag nanoribbon

To make zigzag nanoribbon (zPNR), we have to cut the monolayer in y direction by cutting the bonds which are connecting two phosphorous atoms representing t_2 hopping which can be seen in Fig 1.5. Here, the periodicity is along y direction, so we will have a 1D hamiltonian depending on k_y .

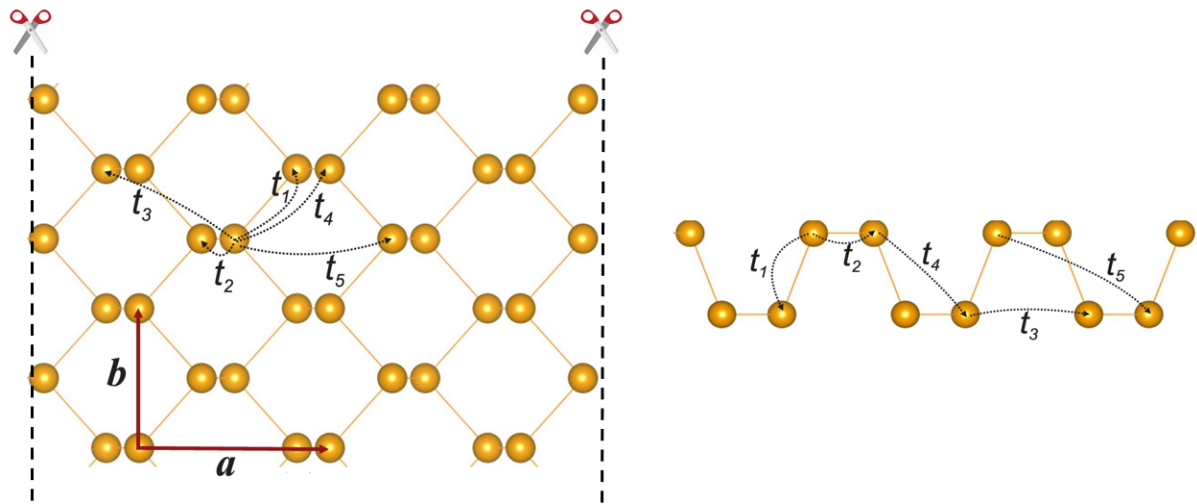


Figure 1.5: This figure shows zPNR having finite length along x axis and having periodicity along y axis in LHS and we have 1 zigzag line on RHS which is the unit cell for our nanoribbon.

It is clear from Fig 1.5 that if the width of our nanoribbon is N then there will be $2xN$ atoms in the unit cell which means $2xN$ bands in the band structure. Now lets talk about Hamiltonians for our nanoribbon.

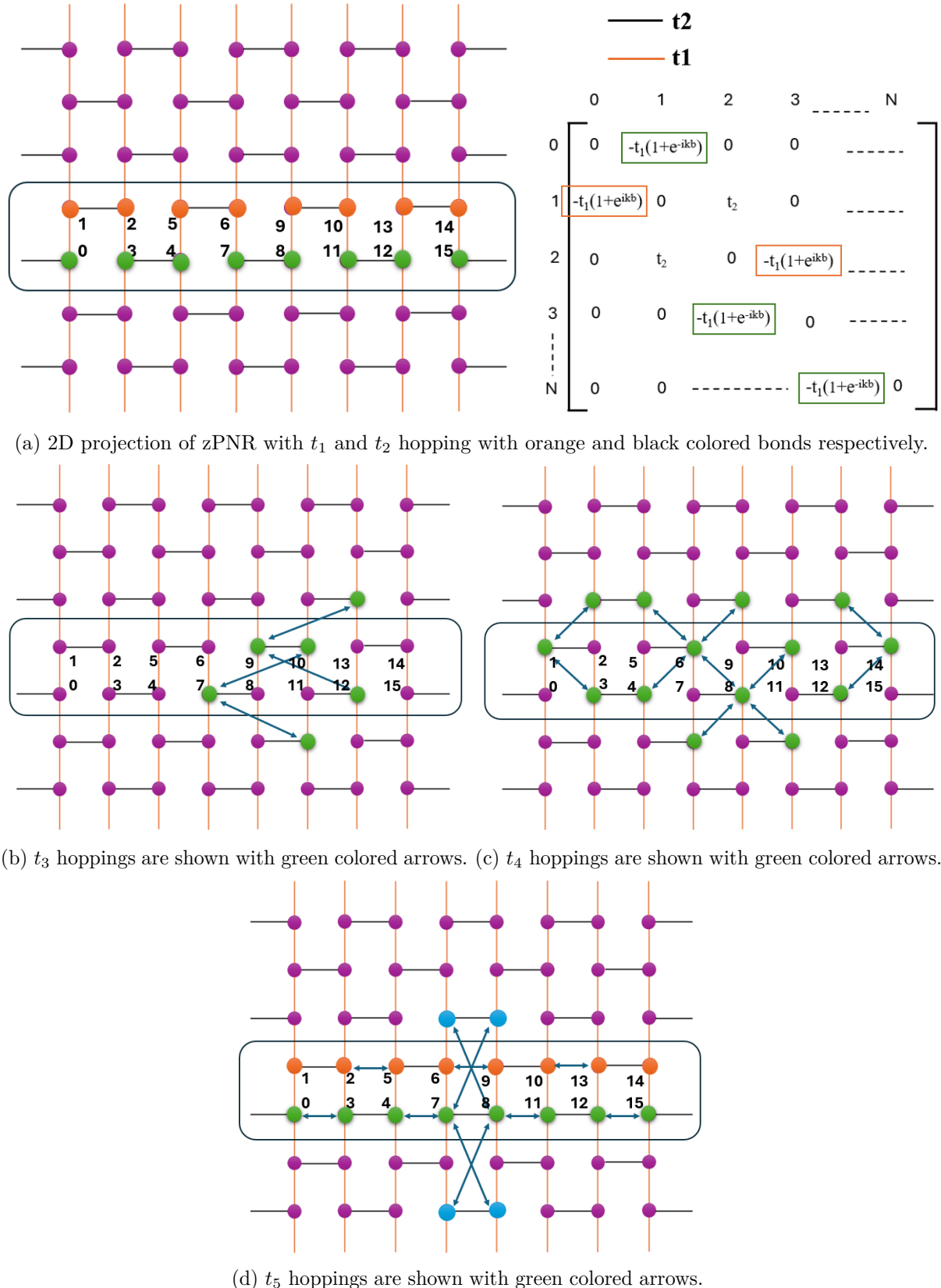


Figure 1.6: These figures explain different hopping integrals we considered for our matrices.

We constructed Hamiltonians for different hopping integrals separately to keep things easier for us and also if something is not working out, then we can check Hamiltonians of different hopping integrals separately to check where we messed up.

In Fig 1.6a, we show the unit cell in black colored box and indexing of the atoms that we considered in our code. We represent t_1 and t_2 hopping integrals by orange and black colored bonds respectively. We have also shown matrix for these two hopping integrals together, in which we see that there is no phase multiplied with t_2 because there is no t_2 hopping between atoms in different unit cells. And for t_1 hopping, matrix elements in orange colored box shows orange atoms hopping with one atom inside the unit cell and one atom outside the unit cell in $+k_y$ direction. Similarly, for matrix elements in green colored box shows green atom hopping with one atom inside the unit cell and one atom outside the unit cell in $-k_y$ direction. Similar considerations can be taken for the construction of matrices of other hopping integrals. To grasp the underlying physics of this model, we delve into the impact of the ratio between the two primary hopping parameters on the electronic structure's behavior for zig-zag phosphorene nanoribbons (zPNRs). Our initial focus is on examining how the ratio $|t_2/t_1|$ and keeping other hopping integrals constant influences the presence of quasi-flat bands and their associated edge states within zPNRs.

To do it, we constructed the matrix for ribbon width(N) = 50 (100 atoms in unit cell). The way we considered these hopping integrals for our matrices are shown in Fig 1.6. Then we added all the matrices and diagonalized (***using np.linalg.eig()***) it on a grid of k_y to get eigen values and plot it with k_y to get our band structure shown in Fig 1.7. We see in Fig 1.7 that with increase in ratio of $|t_2/t_1|$, two middle bands get detached from the bulk bands and come near to fermi level and at $|t_2/t_1| = 3$, they are becoming two fold degenerate. This degeneracy will be lifted for wave vectors near to $k = 0$ in smaller width of zPNR because of the finite electron tunneling between two opposite edges which we will see in Fig 1.17. In Fig 1.7c, we have plotted band structure by keeping $t_4 = 0$ and it has exact flat bands at fermi level which explains the importance of t_4 hopping for bending of these flat bands at $k=0$.

Results show that for $|t_2/t_1| < 2$, we have a trivial band structure but at $|t_2/t_1| > 2$, the detachment of 2 bands suggest a non-trivial topological state where red colored bands are edge states and suggest us that the behaviour of material is different for the bulk and the edges. To confirm it, we will plot the probability amplitude of all sites for these quasi-flat band.

Note- *In the paper which I am replicating [1], they have written 100-zPNR for these band structures instead of 50-zPNR which doesn't look right because they have 100 bands in their plot and as we discussed earlier that for having 100 bands, you need to have 50 as the width (100-zPNR means 200 bands). I discussed with my adviser also and he also agreed with me that there is no unit cell which can give us N bands for N as the width of zPNR. It can be confirmed by checking further plots such as Fig 11 in the paper itself where they are writing 10-zPNR for 20 bands nanoribbon. I mailed the author also but he didn't reply.*

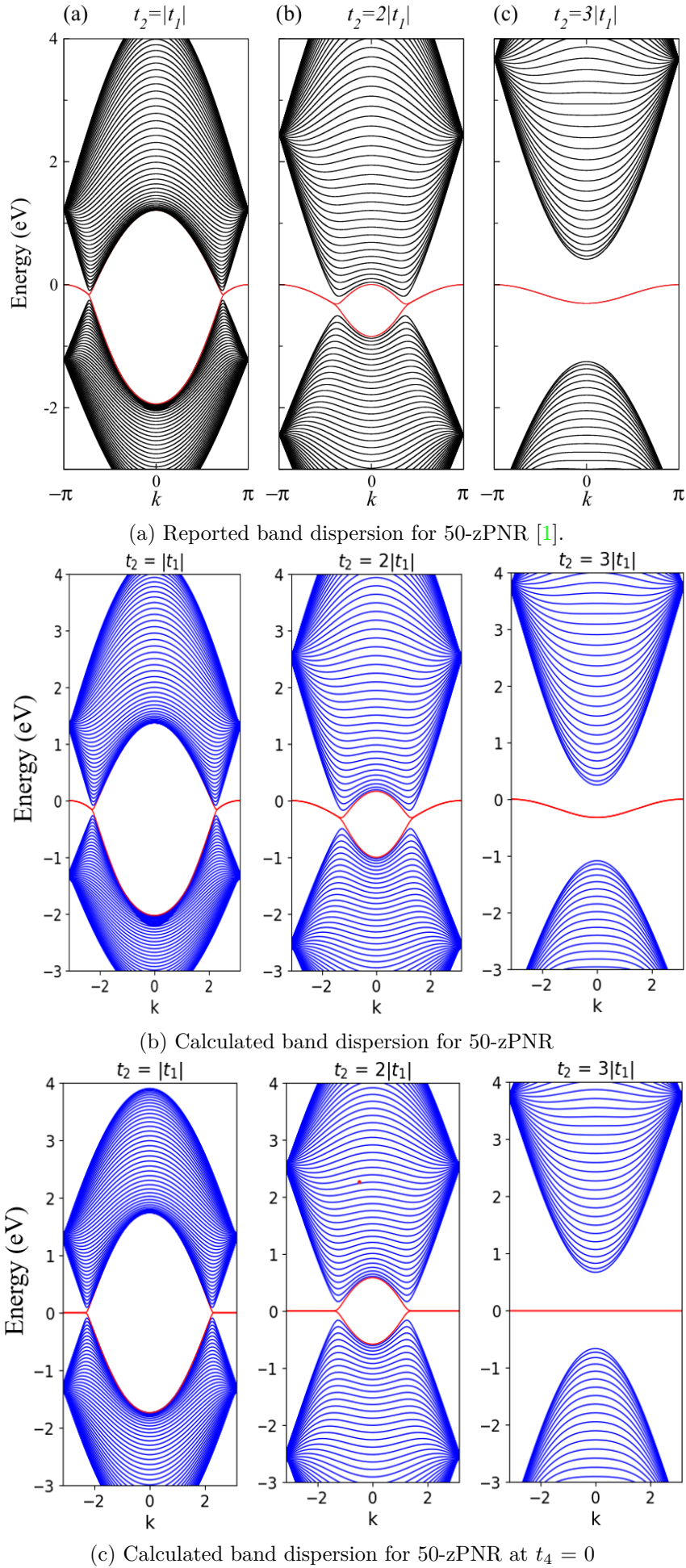


Figure 1.7

Now, we explore probability amplitude of all sites at $k=0$ of these quasi-flat bands. To do this, we have to find eigen vector related to eigen value which represent $k=0$ point of quasi-flat band which will have 100 elements representing coefficients for all 100 sites that we have. And to plot the probability amplitude, we have to plot square of these coefficients vs the site number which can be seen in Fig 1.8.

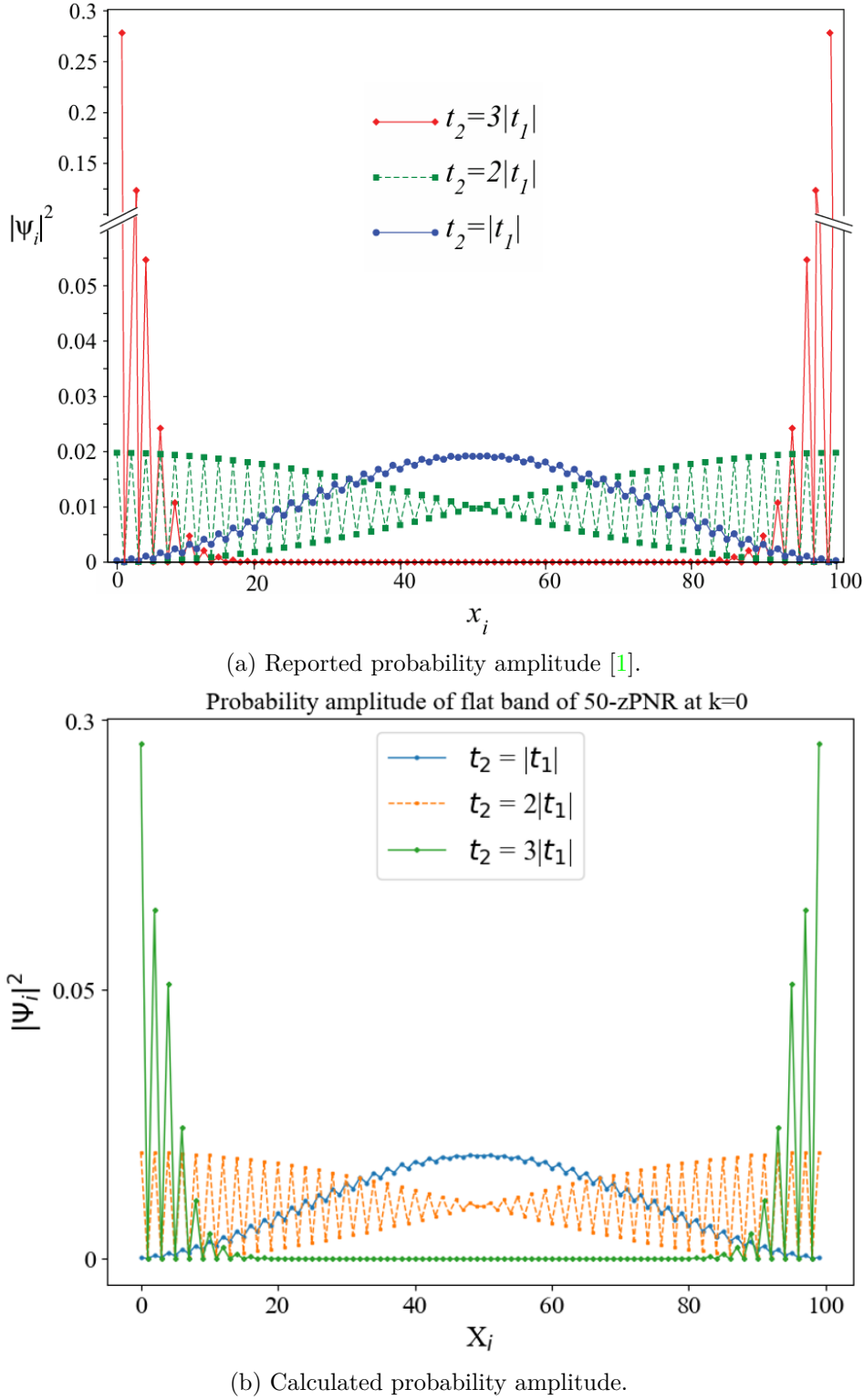


Figure 1.8: This figure shows probability amplitude of sites in flat band at $k = 0$ in 50-zPNR for different ratios of $|t_2/t_1|$ and $t_3, t_4, t_5 = 0$.

As can be clearly seen, for small values of ratio $|t_2/t_1|$, the probability amplitude is large for the bulk sites, whereas for the edge sites, it is minimal or zero. The probability amplitude of the bulk sites decreases as this ratio is increased. For $|t_2/t_1|=3$, only the probability amplitude of the sites near the edges are nonzero, thus indicating the importance of the $|t_2/t_1|$ ratio in the creation of the edge states.

Now to see the effect of ribbon width on probability amplitude, we have plotted it for ribbon width(N) = 6 and 14 for a fixed ratio of $|t_2/t_1|=3$ in Fig 1.9.

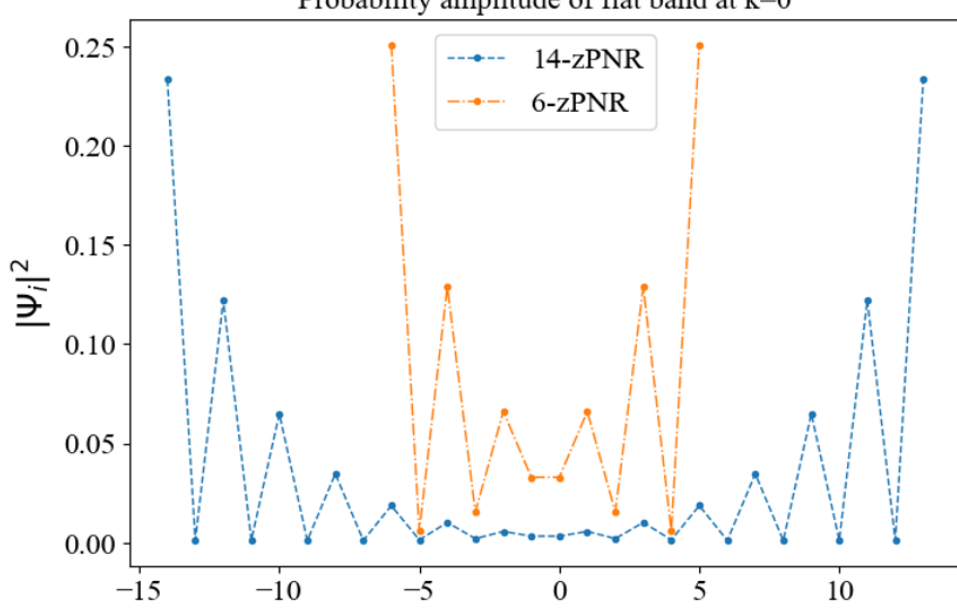
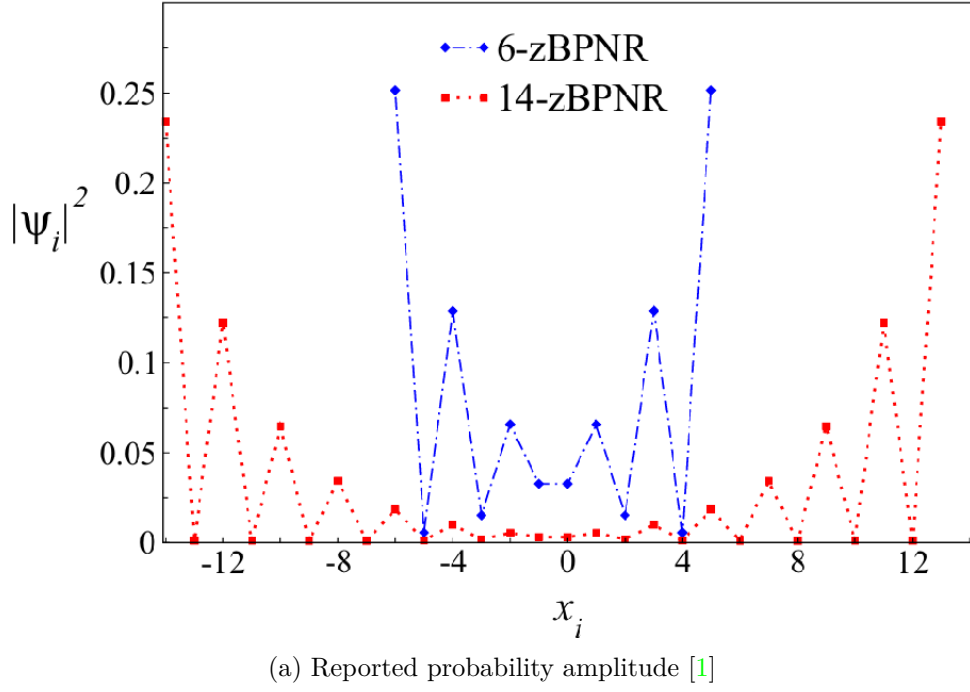


Figure 1.9: This figure shows probability amplitude of sites in flat band at $k = 0$ in 6-zPNR and 14-zPNR for fixed ratio of $|t_2/t_1| = 3$.

Clearly, the ribbon width is also important for the creation of the edge states in zPNRs.

1.3.2 Armchair nanoribbon

To make armchair nanoribbon(aPNR), we have to cut the monolayer in x direction along the bonds which are connecting two phosphorous atoms representing t_2 hopping which can be seen in Fig 1.10. Here, the periodicity is along x direction, so, this time we will have a 1D Hamiltonian depending on k_x .

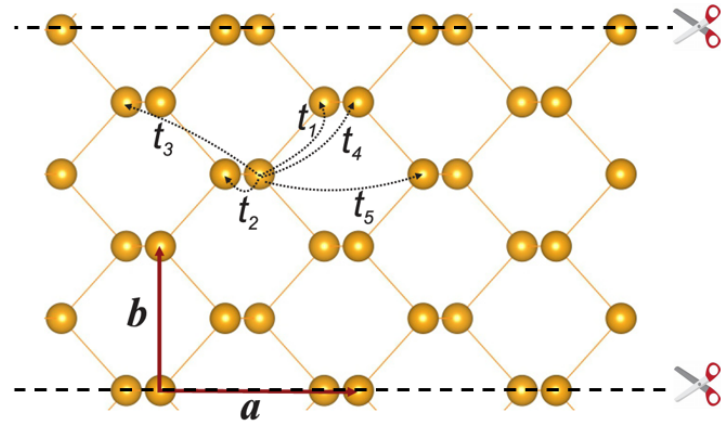


Figure 1.10: aPNR having finite length along y axis and having periodicity along x axis

2D projection of the armchair nanoribbon and indexing of atoms used in code is shown in Fig 1.11. Here again orange bonds represent t_1 hopping integrals and black bonds represent t_2 hopping integrals. This time there is no t_1 hopping outside the unit cell as there was no t_2 hopping in zPNR.

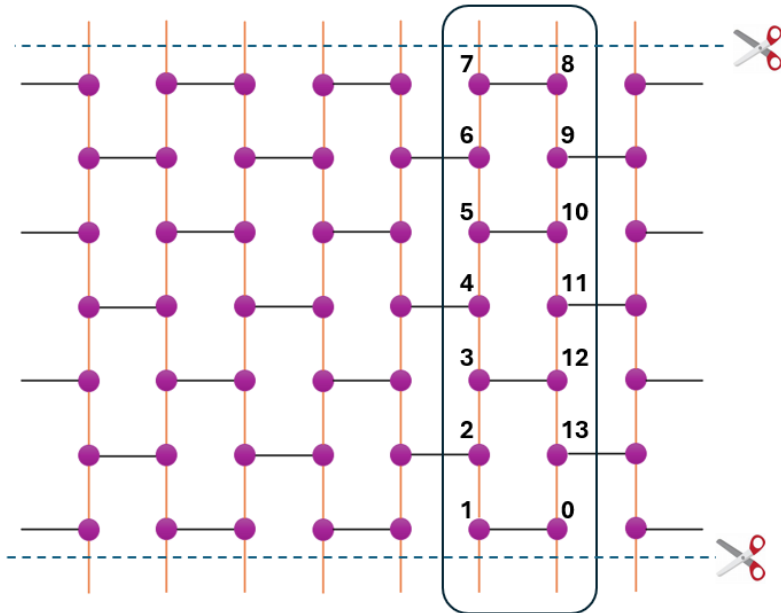
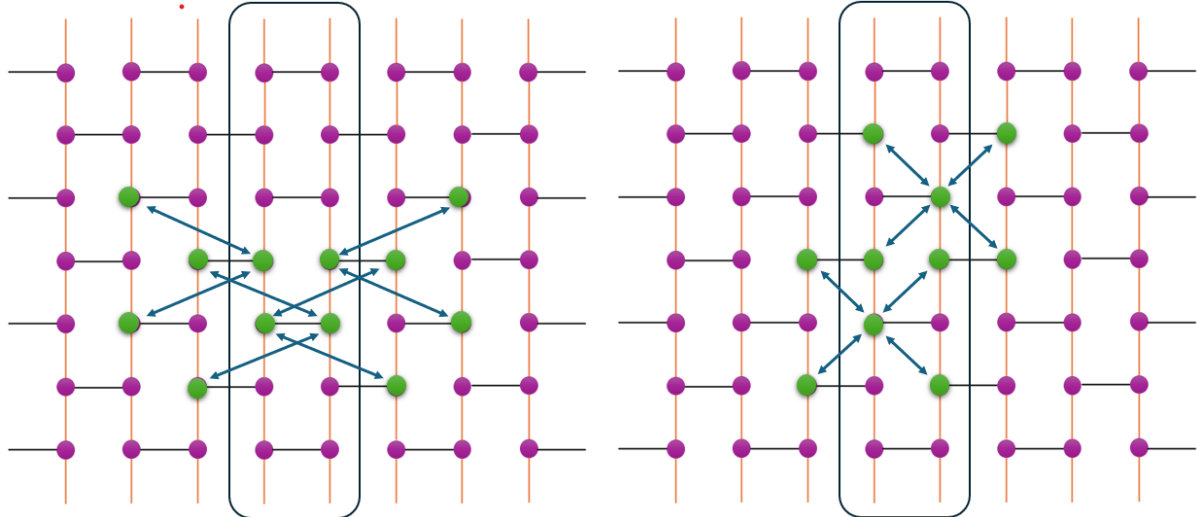
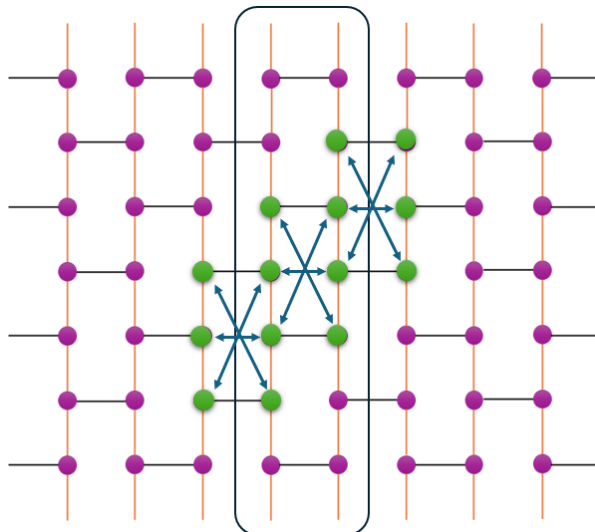


Figure 1.11: 2D projection of aPNR with black colored box showing the unit cell.

The idea is same for aPNR as zPNR, i.e. construction of matrices for different hopping integrals separately. For the sake of completeness, we are adding the images explaining how hopping integrals look in this nanoribbon in Fig 1.12



(a) t_3 hoppings are shown with green colored arrows. (b) t_4 hoppings are shown with green colored arrows.



(c) t_5 hoppings are shown with green colored arrows.

Figure 1.12: This figure explains different hopping integrals we considered for our aPNR matrix.

After constructing the Hamiltonian, we diagonalized it on a grid of k_x and plot the band structure shown in Fig 1.13. Note that the band structures of aPNR for different ratios of $|t_2/t_1|$ were not given in the paper which we are replicating, but 8-aPNR at $|t_2/t_1| = 3$ is given in the paper and here 50-aPNR at $|t_2/t_1| = 3$ is comparable to that band structure. The band structure tells us that armchair nanoribbon doesn't show any non trivial topological state at ratio $|t_2/t_1| > 2$, because there are no edge modes getting detached here. So, it is just a trivial semiconductor.

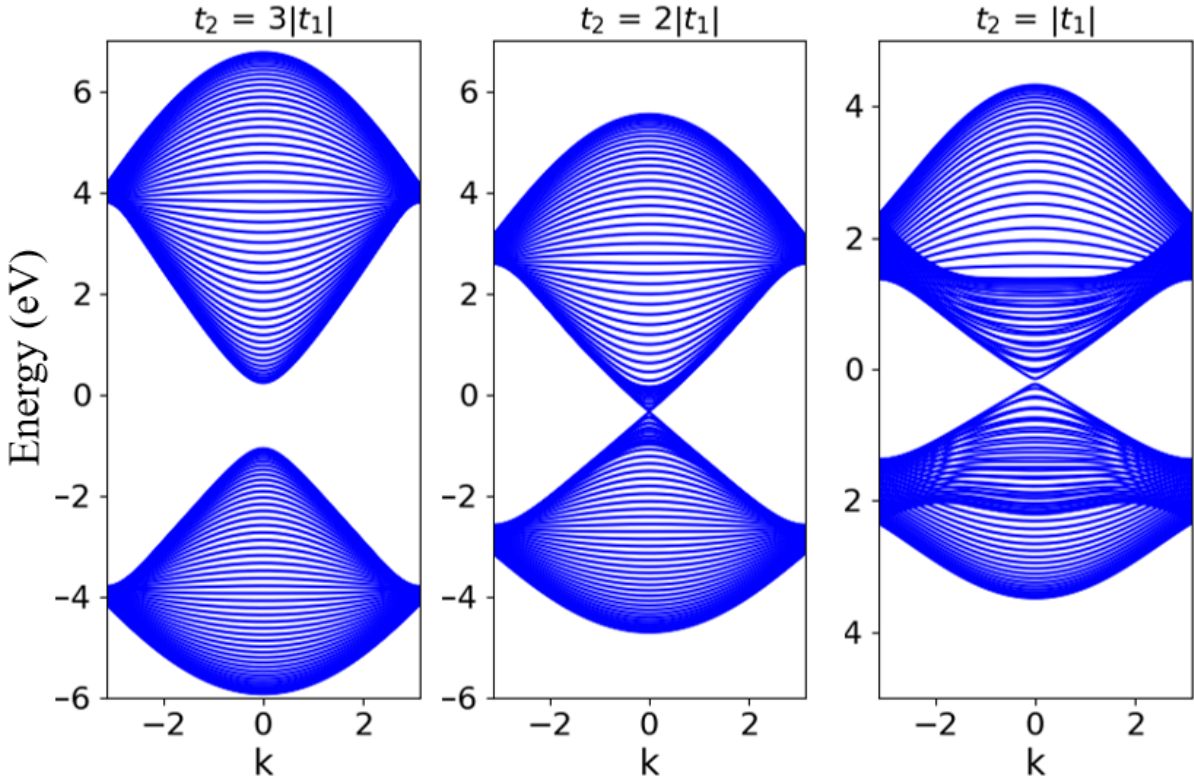


Figure 1.13: Band structure of 50-aPNR for different hopping integrals.

1.4 Effect of in-plane External electric field

Now, we will study the effect of in plane external electric field applied along the ribbon width. To do it, we will make a perturbation matrix which will be a diagonal matrix considering that this electric field is small enough that it will not affect the hopping integrals. This will break the sublattice symmetry of the system because of the different onsite potentials of different sites generated by external electric field.

1.4.1 Response of aPNR to E_{ext}

We know that the potential acting on electron having charge $-e$ by external electric field E_{ext} , at distance d from the source is given by,

$$V_{ext} = -eE_{ext}d \quad (1.10)$$

To construct this diagonal matrix, we took 0^{th} atom as the reference which means $d=0$ for 0^{th} atom and then we found distance of other atoms relative to 0^{th} atom.

Then, we constructed tight binding Hamiltonian of 8-aPNR (16x16) and added it with our perturbation matrix of size 16x16 (16 atoms), and then we diagonalize it to see the effect of E_{ext} on the band structure. Fig 1.14 shows the band structure and probability amplitude of upper valence band and lower conduction band for unperturbed case. We can see that the probability amplitude is distributed in the bulk.

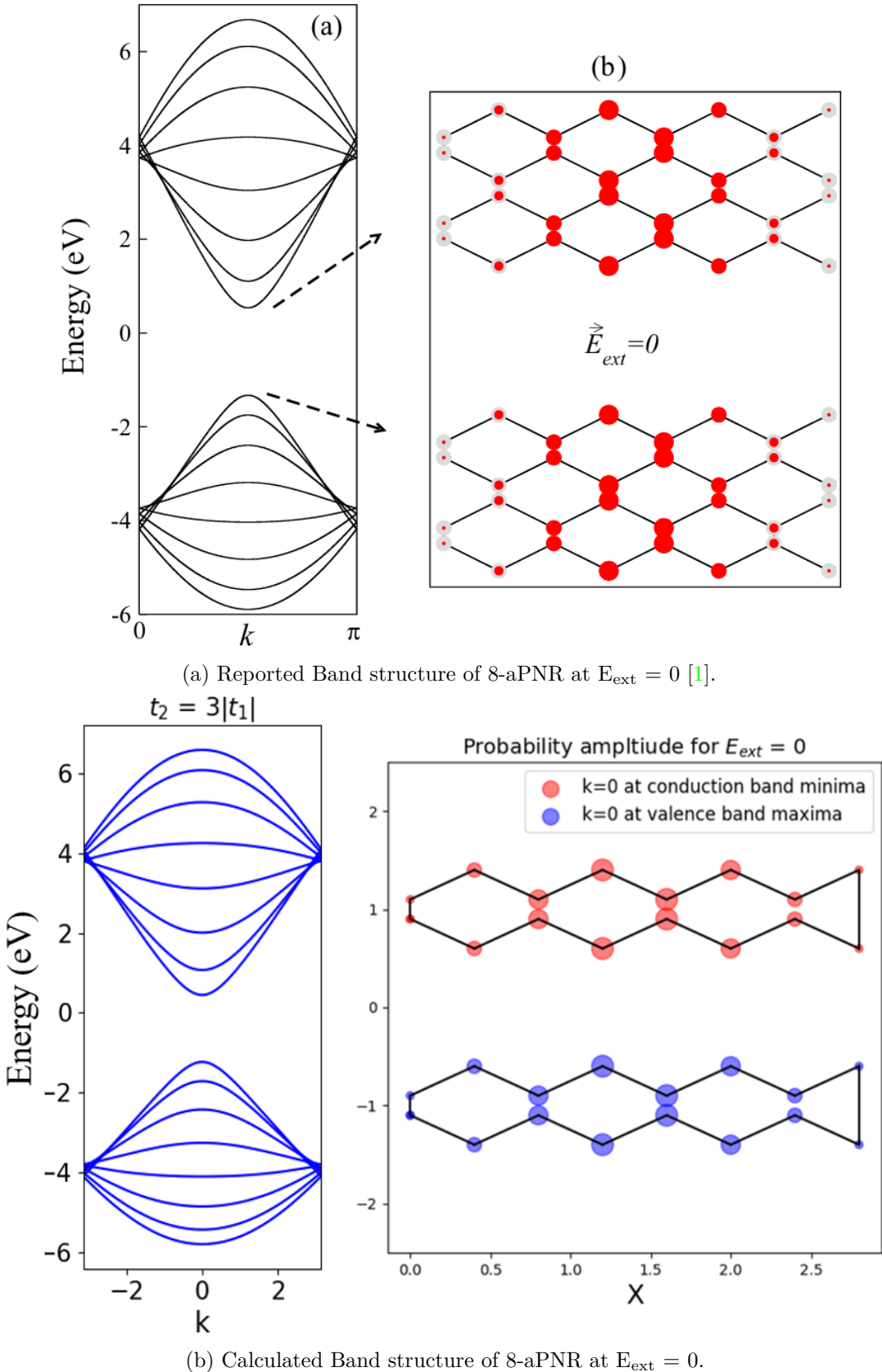
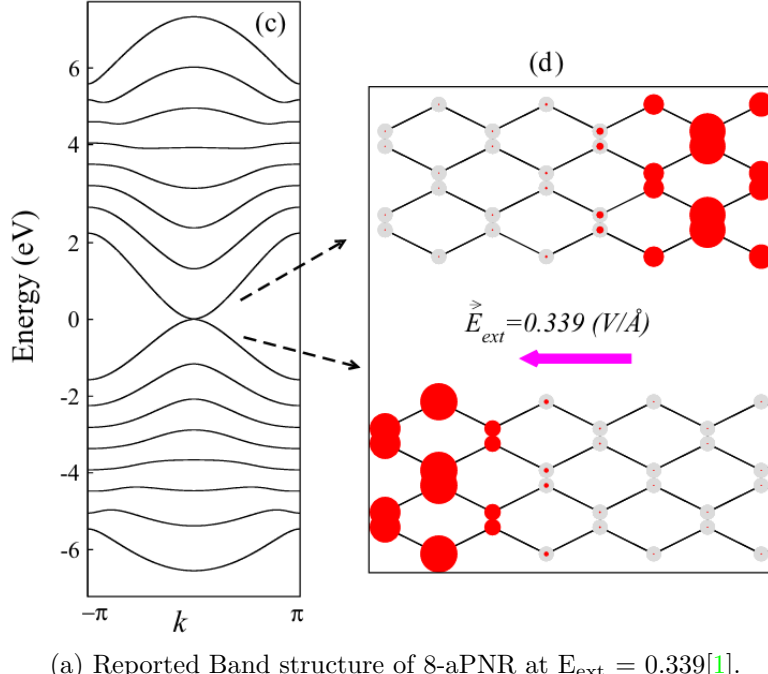


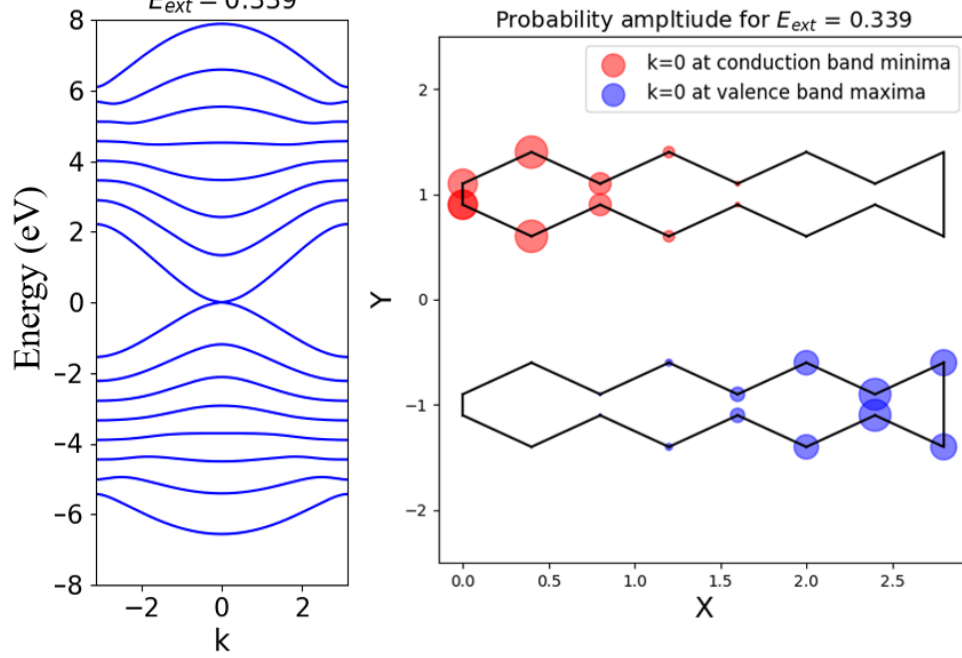
Figure 1.14: This figure represents 8-aPNR band structure and probability amplitude at $E_{ext}=0$.

When a transverse electric field, denoted as E_{ext} , is applied across the width of the nanoribbon, the states associated with the Conduction Band Minimum (CBM),

characterized by positive band curvature (electron states), undergo a downward energy shift due to the Stark effect. Conversely, the Valence Band Maximum (VBM) states (hole states) experience an upward energy shift. Consequently, the CBM and VBM states become localized at the edges of the ribbon, as illustrated in Fig 1.15. With a further increase in the field strength, the two bands progressively approach each other due to the electrostatic potential difference between the opposite edges. This leads to a reduction in the band gap, culminating in its closure at a critical transverse field strength denoted as $E_c = 0.339$ volt/angstrom. We can think this point as an insulator-metal phase transition.



(a) Reported Band structure of 8-aPNR at $E_{ext} = 0.339$ [1].



(b) Calculated Band structure of 8-aPNR at $E_{ext} = 0.339$.

Figure 1.15: This figure represents 8-aPNR band structure and probability amplitude at $E_{ext}=0.339$ volt/angstrom.

Note:- Here, the probability amplitude is shifted in two opposite edges, but reported and calculated shows probability amplitude in two different directions for both CBM and VBM. It is because I considered E_{ext} in opposite direction in my code as compared to shown in reported one.

As discussed, with increase in electric field, band gap decreases in aPNR, but this gap closure of aPNRs with small widths of aPNR exhibits an interesting trend. For instance, for the 8aPNR, the band gap closes for $E_c = 0.339$, it opens again and closes at 0.527 volt/angstrom which can be seen in Fig 1.16. The opening up of the band gap after its closure for very small ribbon widths is related to the finite hopping integrals between the two opposite edges.

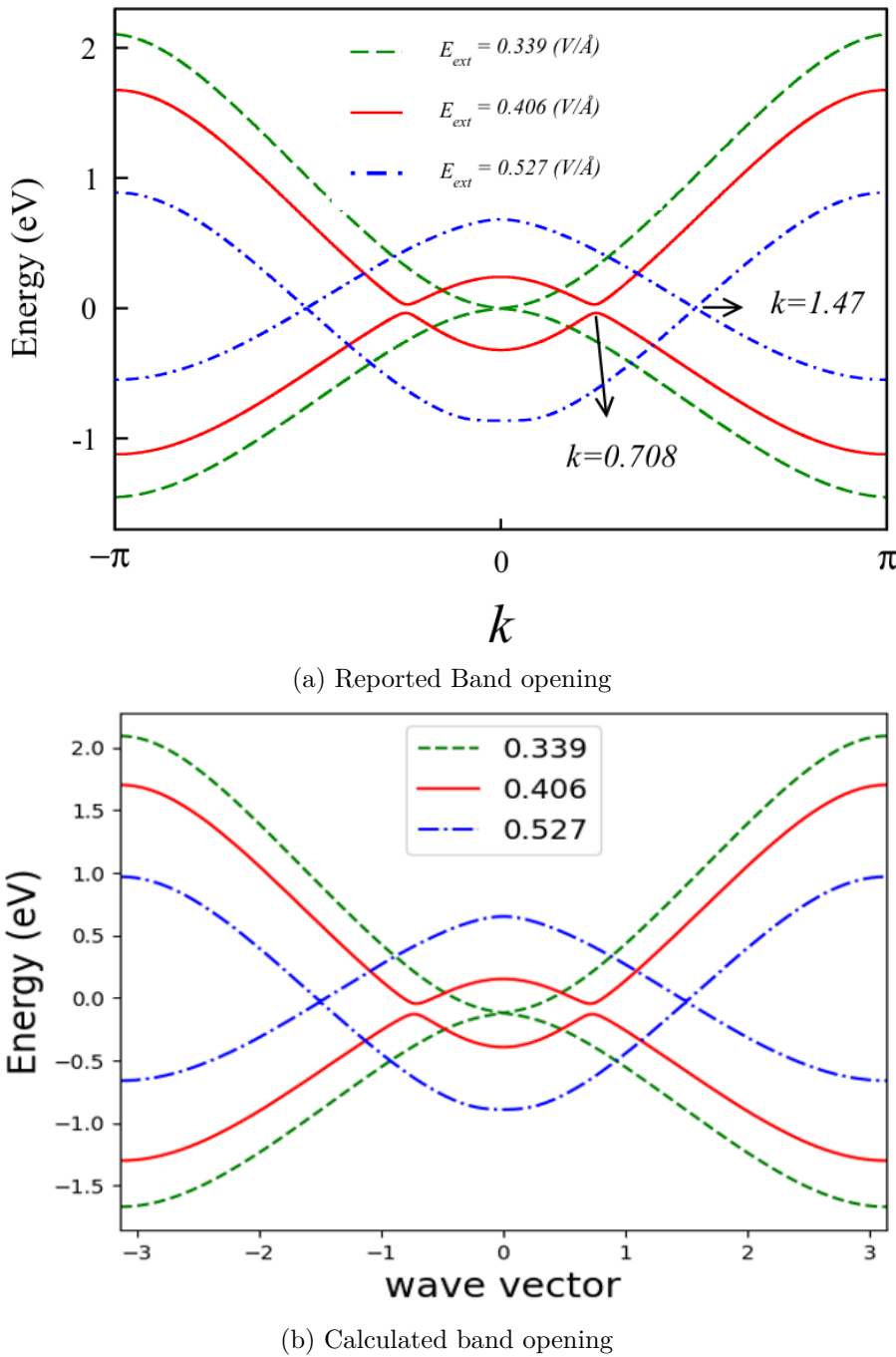


Figure 1.16: Valence band maxima and conduction band minima of 8aPNR for different E_{ext} .

1.4.2 Response of zPNR to E_{ext}

We have to again make a perturbation diagonal matrix here, the diagonal elements will be different as compared to armchair nanoribbon because of different indexing and distance between atoms.

Unlike armchair nanoribbon, here there is not much change in conduction band and valence band, but with increase in E_{ext} , degeneracy of the edge bands get broken for all values of k and wave functions of these upper and lower quasi flat bands are localized on both the opposite edges. These results can be seen in Fig 1.17 and Fig 1.18 for 10-zPNR.

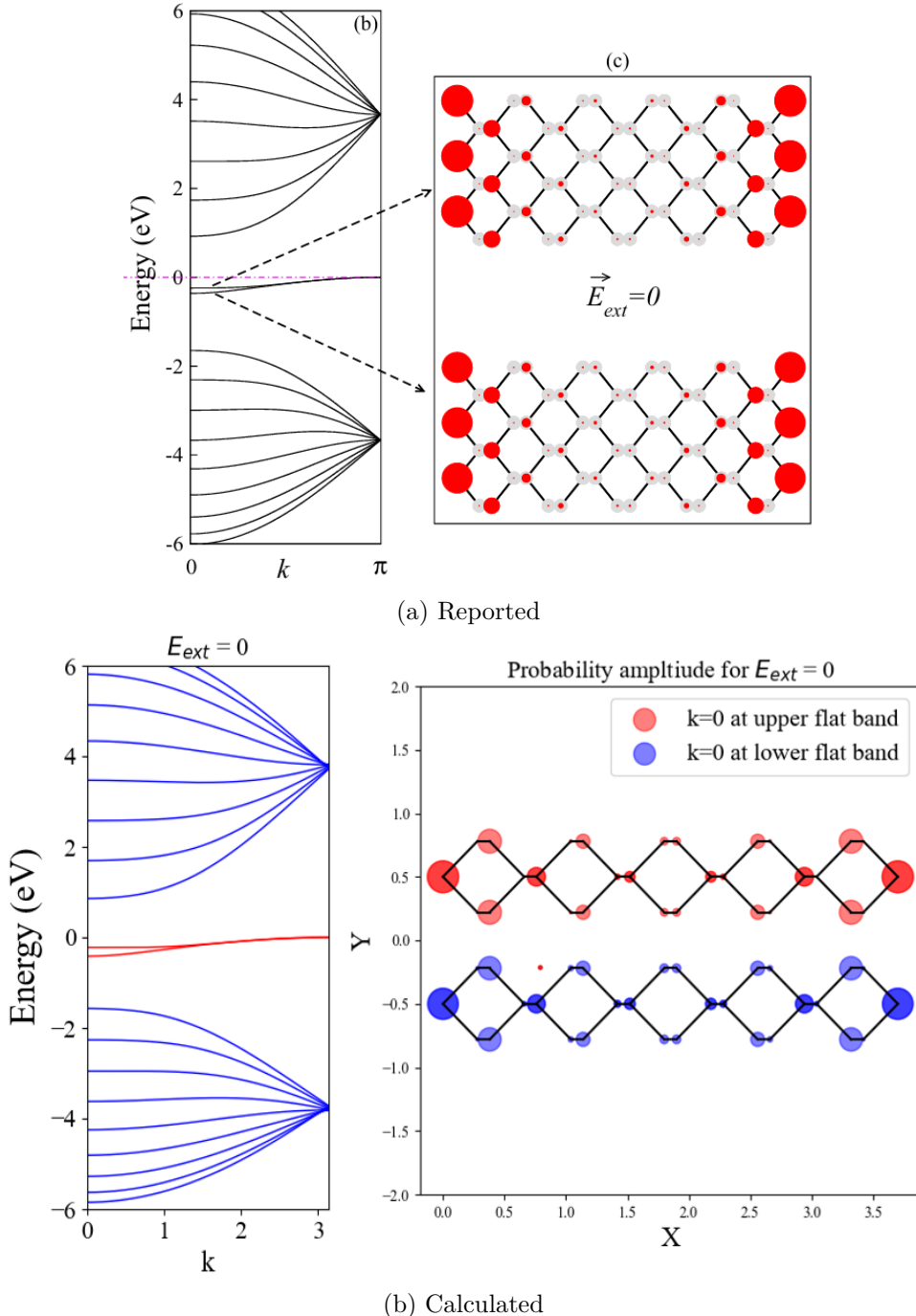


Figure 1.17: This figure represents 10-zPNR band structure and probability amplitude at $E_{\text{ext}}=0$ volt/angstrom.

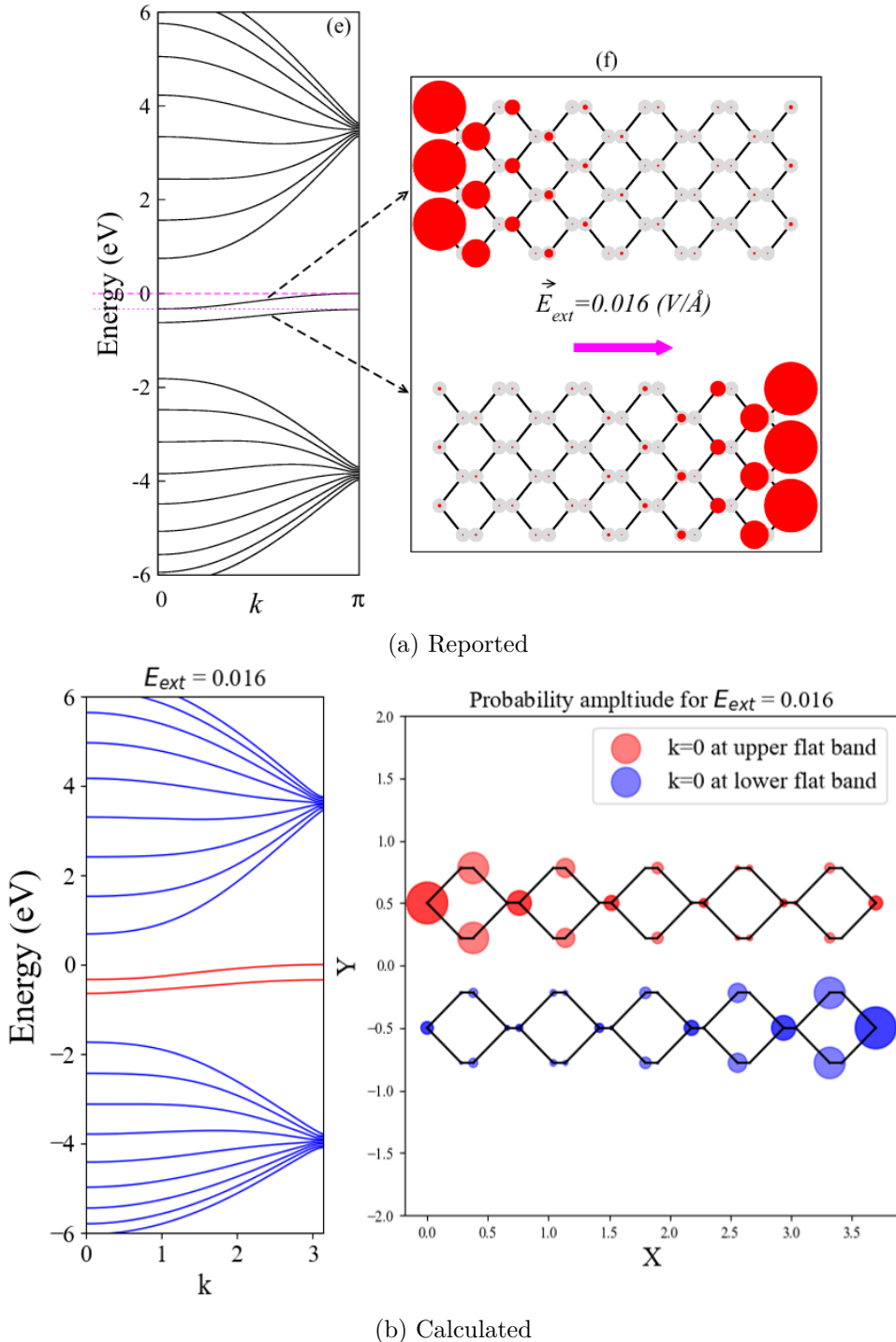


Figure 1.18: This figure represents 10-zPNR band structure and probability amplitude at $E_{ext}=0.016$ volt/angstrom.

Now, by the case of 6-zPNR and 20-zPNR in Fig1.19, we observe that with increase in width size of the nanoribbon, the critical electric field (when quasi-flat bands become parallel) decreases.

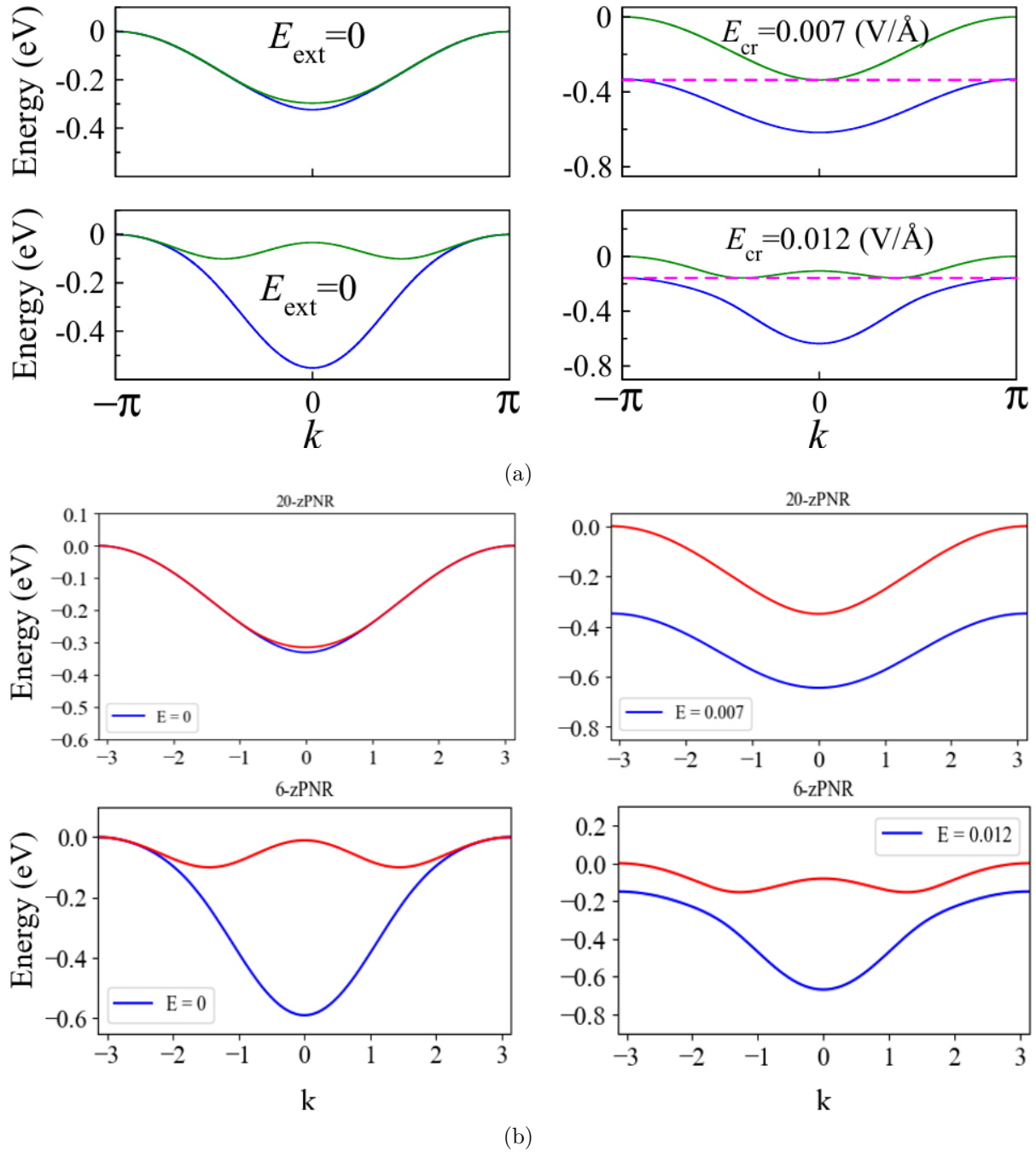


Figure 1.19: (a) Quasi-flat bands for 20-zPNR at $E_{\text{ext}} = 0$ in left and $E_{\text{ext}} = 0.007$ in right (b) Quasi-flat bands for 6-zPNR at $E_{\text{ext}} = 0$ in left and $E_{\text{ext}} = 0.012$ in right

1.5 Quantum transport in zig-zag nanoribbon

Usually we see that the conductance of a 2-dimensional conductor is given by

$$G = \frac{\sigma W}{L} \quad (1.11)$$

where the conductivity σ is a material property, W is the width and L is the length of the conductor.

Small conductors whose dimensions are intermediate between the microscopic and the macroscopic are called mesoscopic. They are much larger than microscopic objects like atoms but not large enough to be “ohmic”. A conductor usually shows ohmic behaviour if its dimensions are much larger than each of three characteristics length scales: (1) the de Broglie wavelength, which is related to Kinetic energy of the electrons, (2) the mean free path, which is the distance that an electron travels before its initial momentum is destroyed and (3) the phase relaxation length, which is the distance that an electron travels before its initial phase is destroyed.

We want to understand the transportation of electron through zigzag nanoribbon which does not show ohmic behaviour because of its finite width and take over of quantum properties. Landauer expressed the current through a conductor in terms of the probability that an electron can transmit through it. We are going to use Landauer-Buttiker formalism to calculate the transmission of electrons which is based on the recursive Green's function technique. We start with explaining this formalism for a simple lattice arrangement which is a 2D square lattice. Then we will move to our system which is zigzag nanoribbon.

1.5.1 Landauer-Buttiker Formalism for square lattice

In this method, we consider a two terminal device consisting of left lead, scattering region, and right lead as shown if Fig 1.20.

Consider the square-lattice two-dimensional two-terminal device shown in Fig 1.20. The left and right leads are shown, along with the device region. Let the number of sites in the device region be $n_x \times n_y (=N)$. Let us call the number of sites in the lead, which couple to the device region, nsf. In this particular case of square lattice $nsf = n_y$.

We begin by focusing on the left lead and constructing the Hamiltonian for a single unit cell, denoted as α_L

$$\alpha_L = \begin{pmatrix} e_L & t_L & 0 & 0 \\ t_L & e_L & t_L & 0 \\ 0 & t_L & e_L & t_L \\ 0 & 0 & t_L & e_L \end{pmatrix} \quad (1.12)$$

where e_L is the onsite energy (0 in our case) for the atoms in the left lead and t_L is the nearest neighbour hopping strength.

Similarly, considering only the nearest neighbour hopping, the coupling between the unit cells can be written as

$$\beta_L = \begin{pmatrix} t_L & 0 & 0 & 0 \\ 0 & t_L & 0 & 0 \\ 0 & 0 & t_L & 0 \\ 0 & 0 & 0 & t_L \end{pmatrix}. \quad (1.13)$$

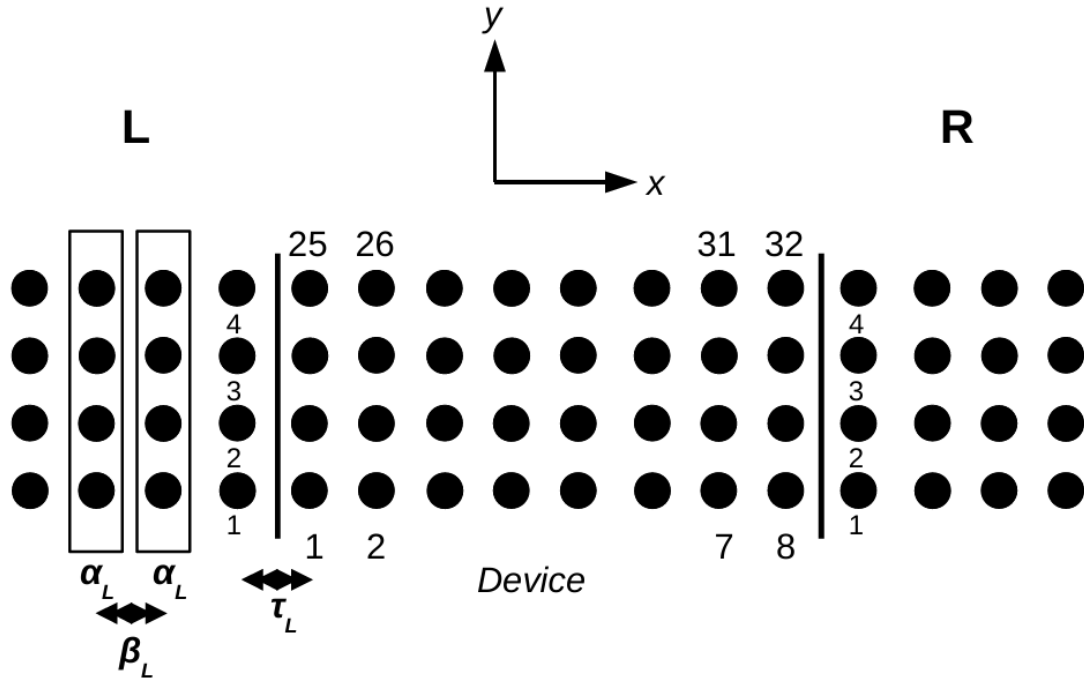


Figure 1.20: Setup for calculating the two terminal transmission. The rectangles indicate the unit cell for the leads and each unit cell is coupled to the next by β .

Once, we have α_L and β_L matrices we can use Dyson's equation to get the surface Green's function ($g_{s,L}$) for the left lead.

$$g_{s,L} = \left[(E + i0^+) I - \alpha_L - \beta_L^\dagger g_{s,L} \beta_L \right]^{-1}, \quad (1.14)$$

where E is the energy of the incident electron and we have added a small positive imaginary number to the energy E at which the equation is being evaluated and I is the identity matrix of size $nsf \times nsf$. We also need a first approximation to the surface Green's function, $g_{s,L}^0$. It can be chosen to be

$$g_{s,L}^0 = \left[(E + i0^+) I - \alpha_L \right]^{-1}. \quad (1.15)$$

The iterative procedure can be continued till a desired level of accuracy is achieved. The criteria for convergence we used was the absolute sum of matrix elements of the matrix which is the difference of two consecutive matrices of Dysons's equation. An identical procedure can be applied to get the surface Green's function ($g_{s,R}$) for the right lead. In this case,

$$\alpha_R = \begin{pmatrix} e_R & t_R & 0 & 0 \\ t_R & e_R & t_R & 0 \\ 0 & t_R & e_R & t_R \\ 0 & 0 & t_R & e_R \end{pmatrix}, \quad (1.16)$$

where e_R is the onsite energy (0 in our case) for the atoms in the right lead and t_R is the nearest neighbour hopping strength.

Further,

$$\beta_R = \begin{pmatrix} t_R & 0 & 0 & 0 \\ 0 & t_R & 0 & 0 \\ 0 & 0 & t_R & 0 \\ 0 & 0 & 0 & t_R \end{pmatrix}. \quad (1.17)$$

Similar to the left lead, we have

$$g_{s,R} = [(E + i0^+) I - \alpha_R - \beta_R^\dagger g_{s,R} \beta_R]^{-1}, \quad (1.18)$$

and the initial approximation to the surface Green's function is

$$g_{s,R}^0 = [(E + i0^+) I - \alpha_R]^{-1}. \quad (1.19)$$

Note:- We added a small positive imaginary number in the iterative process to maintain the stability of iteration because in case of very small determinant, surface Green's function will diverge and addition of imaginary number can give some magnitude to determinant. Smaller this number is, convergence will be harder.

The coupling between the leads and the device is given by the coupling matrices τ_L and τ_R . If we consider only the nearest neighbour hopping between the leads and the device, with strengths tc_L and tc_R , for the left and the right leads, respectively, then $\tau_{L,R}$ are matrices of dimension $N \times nsf$. The non-zero elements in this particular setup are given by

$$\tau_L(1,1) = \tau_L(9,2) = \tau_L(17,3) = \tau_L(25,4) = tc_L \quad (1.20)$$

$$\tau_R(8,1) = \tau_R(16,2) = \tau_R(24,3) = \tau_R(32,4) = tc_R \quad (1.21)$$

Now, using the surface Green's functions and the coupling matrices, we can calculate the self-energy matrices (Σ_L and Σ_R) for the left and right leads. This completes the process of replacing the semi-infinite leads by finite matrices.

$$\Sigma_L = [\tau_L]_{N \times nsf} [g_{s,L}]_{nsf \times nsf} [\tau_L^\dagger]_{nsf \times N} = [\Sigma_L]_{N \times N} \quad (1.22)$$

$$\Sigma_R = [\tau_R]_{N \times nsf} [g_{s,R}]_{nsf \times nsf} [\tau_R^\dagger]_{nsf \times N} = [\Sigma_R]_{N \times N} \quad (1.23)$$

Next, we need to specify the Hamiltonian H , for the device region. This is straightforward, if we consider only the nearest neighbour hopping and onsite energies. Ultimately, the retarded Green's function for the system is obtained by

$$G^r = [(E + i0^+)I - H - \Sigma_L - \Sigma_R]^{-1} \quad (1.24)$$

where I is now a $N \times N$ identity matrix. The broadening matrices Γ_L and Γ_R are related to the imaginary part of the self-energy matrices,

$$\Gamma_L = i[\Sigma_L - \Sigma_L^\dagger] \quad (1.25)$$

$$\Gamma_R = i[\Sigma_R - \Sigma_R^\dagger] \quad (1.26)$$

Thus, the effect of the leads is two-fold; first the real part of the self-energy changes the eigenvalues and eigenstates of the system and further it introduces an imaginary part to

the energy, which leads to the broadening of the energy levels (hence the name broadening matrices!). Now, finally, we can obtain the transmission coefficient,

$$T(E) = \text{trace}(\Gamma_L G^r \Gamma_R G^{r\dagger}) = \text{trace}(\Gamma_R G^r \Gamma_L G^{r\dagger}) \quad (1.27)$$

After calculating the Transmission, conductance(σ) can be calculated by

$$\sigma = \frac{e^2}{h} T(E) \quad (1.28)$$

Note: In the results below, we calculated Transmission on a grid of Energy. And they were taking some time, so, we distributed this grid in 8 different processors (parallelisation).

1.5.2 Transmission in Square Lattice arrangement

The accurate integer quantization of transmission observed in Fig 1.21 can verify the credibility of the formalism discussed above and ensure us that our code is working fine. We keep our convergence criteria as absolute sum of matrix elements of difference of two consecutive matrices of Dyson's equation, $a = 10^{-3}$ and the positive imaginary number $n = 10^{-3}i$.

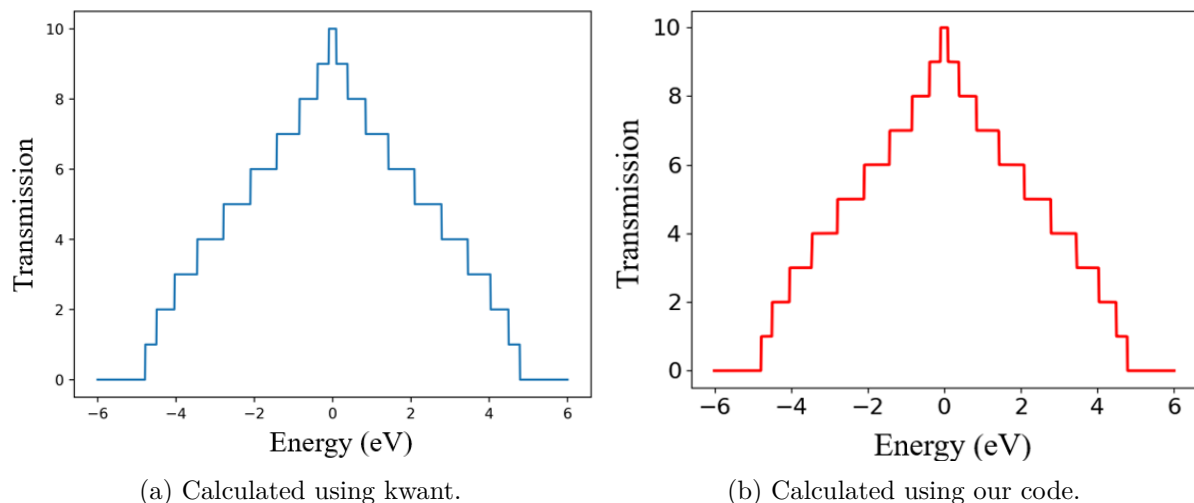


Figure 1.21: This figure represents Transmission of electrons having energy E in square lattice.

1.5.3 Transmission in 10-zPNR

The setup for two terminal transmission for 10-zPNR is shown in Fig 1.22. The idea is similar to square lattice. But instead of nearest neighbour hopping integral only, we will have to consider 5 nearest neighbour hopping integrals as discussed earlier also. And in both device and leads, we have to keep 10-zPNR as shown in Fig 1.22. Note that lattice arrangement has translation symmetry (periodicity) along x direction and it is finite along y direction which is a known property of zPNR and this makes our leads semi-infinite. So, by employing the same formalism, we calculate electronic transport in 10-zPNR which is shown in Fig. 1.23.

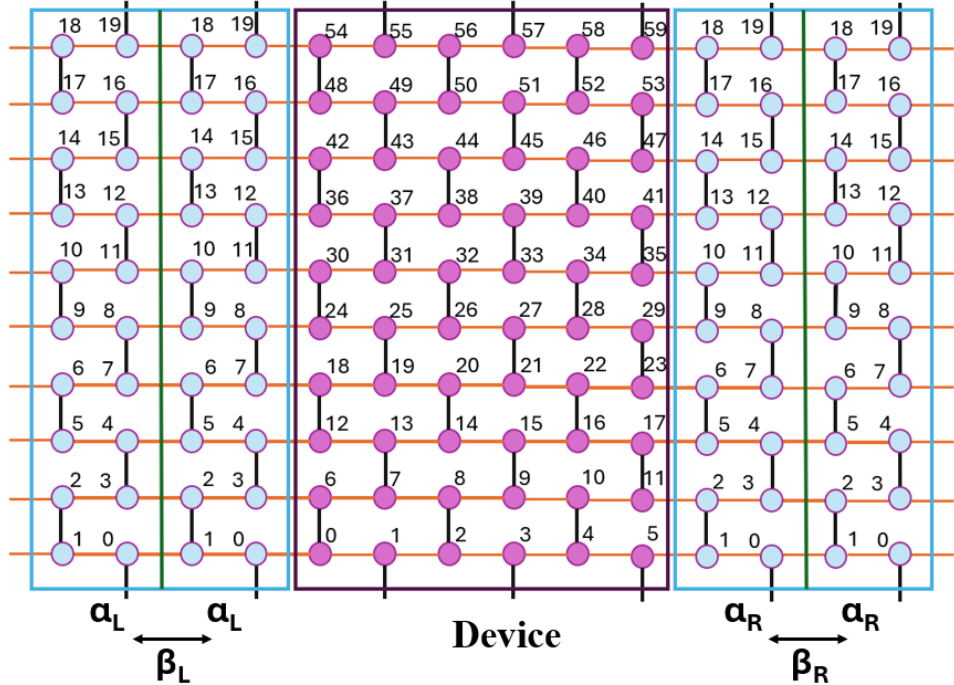


Figure 1.22: Setup for calculating the two terminal transmission for 10-zPNR.

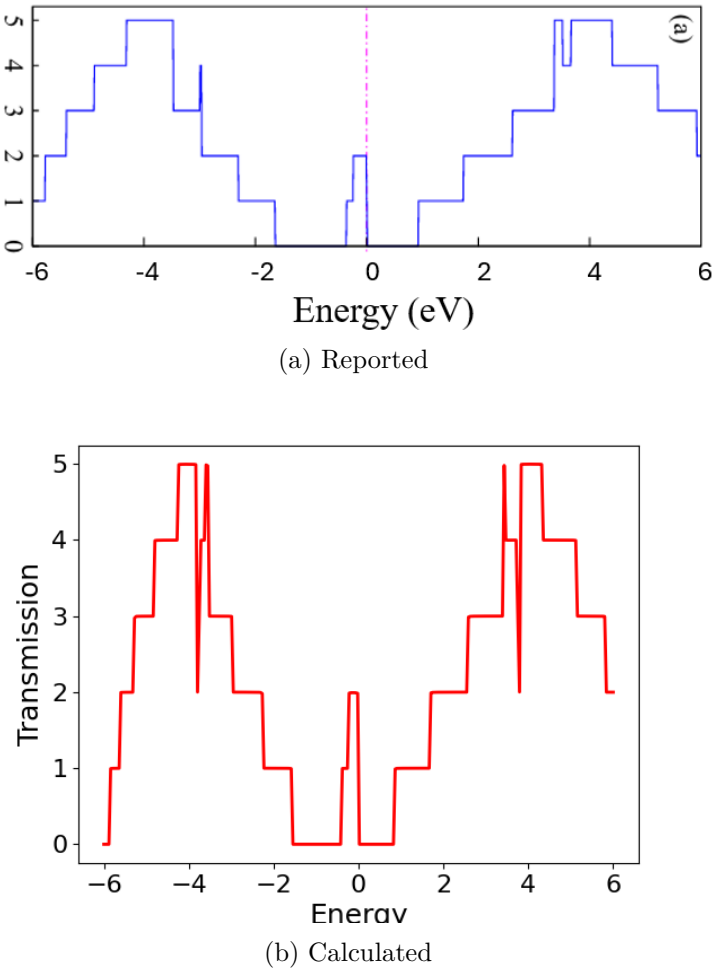


Figure 1.23: This figure represents Transmission of electrons having energy E in 10-zPNR.

1.6 Conclusion

In this study, we have presented numerical findings regarding the band structure and quantum conductance of zig-zag phosphorene nanoribbons (zPNRs) and armchair phosphorene nanoribbons (aPNRs), employing a five-parameter tight-binding (TB) model. We saw the emergence of a relativistic band dispersion along the armchair direction in four band model. Specifically, our numerical simulations for zPNRs unveiled a pair of degenerate quasi-flat bands situated at the Fermi level, localized along the ribbon edges. Notably, this degeneracy was lifted for narrower ribbons due to finite interactions among the edge states.

For aPNRs, a semiconducting behavior was predicted, with the potential for an insulator-metal transition upon the application of a transverse electric field. In zPNRs, an external transverse electric field was applied to eliminate the overlap between quasi-flat bands.

Towards the conclusion of our investigation, our attempts to compute the electron transmission in a 10-zPNR device configuration, including the leads, yielded satisfactory results.

Bibliography

- [1] Esmaeil Taghizadeh Sisakht, Mohammad H Zare, and Farhad Fazileh. “Scaling laws of band gaps of phosphorene nanoribbons: A tight-binding calculation”. In: *Physical Review B* 91.8 (2015), p. 085409.
- [2] Mitsutaka Fujita et al. “Peculiar localized state at zigzag graphite edge”. In: *Journal of the Physical Society of Japan* 65.7 (1996), pp. 1920–1923.
- [3] Motohiko Ezawa. “Topological origin of quasi-flat edge band in phosphorene”. In: *New Journal of Physics* 16.11 (2014), p. 115004.